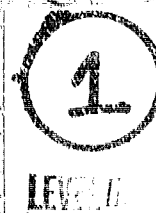


USAAVRADCOM  
TR 78-36

NASA  
Technical Paper 1378

AVRADCOM  
Technical Report 78-36



AD-A067 651

## Performance of a Nasvytis Multiroller Traction Drive

Stuart M. Loewenthal, Neil E. Anderson,  
and Algirdas L. Nasvytis

NOVEMBER 1978

DDC  
RECORDED  
17 APR 1979  
RECEIVED  
VE

DISTRIBUTION STATEMENT A  
Approved for public release  
Distribution unlimited

NASA

NASA  
Technical Paper 1378

AVRADCOM  
Technical Report 78-36

## Performance of a Nasvytis Multiroller Traction Drive

Stuart H. Loewenthal  
*Lewis Research Center, Cleveland, Ohio*

Neil E. Anderson  
*Propulsion Laboratory, AVRADCOM Research and Technology Laboratories  
Lewis Research Center, Cleveland, Ohio*

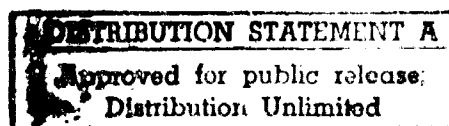
Algirdas L. Nasvytis  
*Transmission Research, Inc., Cleveland, Ohio*

**NASA**

National Aeronautics  
and Space Administration

Scientific and Technical  
Information Office

1978



ACCESSION for	
NTIS	White Section <input checked="" type="checkbox"/>
DDC	Buff Section <input type="checkbox"/>
UNANNOUNCED	<input type="checkbox"/>
JUSTIFICATION	
by	
DISTRIBUTION/AVAILABILITY CODES	
Dist.	AVAIL. and/or SPECIAL
A	

TSARCOM  
STINFO & RLF LIB

## SUMMARY

Parametric tests were conducted on a high-speed, 14.7-to-1 fixed-ratio Nasvytis Multiroller Traction Drive. The test drive was arranged in a single-stage, planetary configuration with two rows of stepped planet rollers contained between the concentric sun and ring rollers. The drive was equipped with an automatic roller-loading mechanism that maintained a constant design traction coefficient. Two drives were tested concurrently in a back-to-back arrangement - one functioning as a speed increaser, the other as a speed reducer. A synthetic, cycloaliphatic traction fluid was the test lubricant. Test parameters included nominal sun-roller speeds to 73 000 rpm and input power levels to 127 kW (170 hp). Three design traction coefficients - namely, 0.039, 0.048, and 0.057 - were tested by varying the geometry of the automatic roller-loading mechanism.

Both the speed increaser and reducer operated smoothly and efficiently through the full range of test conditions. A nominal peak efficiency of 95 percent was measured. Transmission efficiency increased with the applied torque but varied relatively little with changes in operating speed. Varying the design traction coefficient had a relatively small effect on efficiency, creep rate, or operating temperatures. However, with a traction coefficient of 0.057, both drives showed signs of impending slip at high torque and sun-roller speeds greater than 57 500 rpm. Both test drives exhibited good speed regulation, with speed efficiencies greater than 98.4 percent.

## INTRODUCTION

The development of practical, cost-competitive traction drives for a variety of commercial applications, from machine tools to automotive transmissions, is a rapidly expanding field. Although presently about a dozen companies in the United States market traction drives (ref. 1), their widest acceptance has been in Europe, where thousands are in commercial service. Interest is also remarkably high in Japan and the Soviet Union. The majority of these commercial drives are limited to light-duty applications, less than 11 kW (15 hp) (ref. 1).

Because of the high contact stresses associated with high power transfer, many of these traction drives must be unattractively large in order to meet reasonable industrial service life requirements. Progress is being made in developing more compact drives by using cleaner vacuum-processed bearing steels with greater fatigue resistance and traction lubricants with improved tractive properties (ref. 2).

Traction drives combine the potential of smooth, quiet, highly efficient (> 90 percent) power transfer and reliable operation at extremely high speeds (>110 m/sec (20 000 ft/min), ref. 3). Unlike power transmission with gear teeth - which, even when perfectly machined, will generate significant torsional oscillations as the load transfers between teeth - power transmission through traction is inherently smooth and quiet. The tangential compliance of the thin elastohydrodynamic lubricant film between contacting rollers, together with the elastic compliance of the rollers themselves, provides an effective damping action to further reduce vibrational disturbances. Because of their smooth power-transfer characteristics, traction drives often prove to be a cheaper and quieter alternative to high-speed, high-precision planetary gear sets. An example of this is given in reference 4, which reports the design and construction of a simple planetary traction speed reducer. It was designed to replace a precision planetary gear set for a 50 000-rpm pneumatic head on a vertical grinder. The traction drive was not only quieter and smoother running, but also less expensive to manufacture.

Although the concept of power transfer by traction appears, in principle, to be straightforward, the physical mechanisms involved and the proper design criteria to be followed are not well established. The interaction of the lubricant with the nonideal (rough) roller surfaces under the combination of high contact pressures and high lubricant shear rates is extremely difficult to model analytically. For the most part, practical design information for traction contact has been empirically obtained on a particular contact geometry for a specific range of test conditions.

Some of the earliest investigations into traction contact phenomena as they relate to traction drives were conducted by Lubomyr Hewko (refs. 5 to 7). Hewko obtained traction and efficiency performance data for roller contacts of several geometries over a wide range of operating conditions for several lubricants (ref. 5). He varied such parameters as rolling velocity, normal load, temperature, and speed ratio (ref. 5). Hewko later extended much of these data to roller contacts that operate at very high surface speeds (to 127 m/sec (25 000 ft/min)) (ref. 6). Much of this test information served as a data base for the construction of several fixed-ratio, simple planetary traction drives. One of these planetary traction drives, of 3.5-to-1 ratio, was tested against a planetary geared drive of similar size, ratio, and power capacity (ref. 7). The planetary traction drive had significantly higher part-load efficiency and a lower noise signature than the comparable planetary geared drive.

Generally, a single-stage, simple planetary traction drive has a practical speed-ratio limit of about 7. Above this speed ratio the size of the sun roller relative to the ring roller becomes so small as to unfavorably overload the sun-roller contact for appreciable power transfer. A remedy to the speed-ratio limit of single-stage planetary traction drives was devised by A. L. Nasvytis (ref. 3). His drive system uses the

sun and ring rollers of the simple planetary traction drive; but, instead of a single row of constant-diameter planet rollers, Nasvytis substituted two or more rows of "stepped" (or dual diameter) planet rollers. With this new "multiroller" arrangement, practical speed ratios as high as 150 could be obtained in a single stage with three rows of planet rollers. In addition to the immediate size, weight, and simplicity benefits of a high-ratio, single-stage drive, the Nasvytis Multiroller Traction Drive also minimizes the need for bearings by restricting their use to only the last row of planet rollers and either the ring or sun roller.

In reference 3, Nasvytis reports the test results for several versions of his multiroller drive. The first drive tested was a 373-kW (500-hp) torpedo drive of three-planet-row construction with a reduction ratio of 48.2 and an input speed of 53 000 rpm. The outside diameter of the drive itself was 43 cm (17 in.), and it weighed just 930 N (210 lb) with a lightweight magnesium housing. It demonstrated a mechanical efficiency above 95 percent with sun-roller surface speeds greater than 86.4 m/sec (17 000 ft/min, ref. 3). To investigate ultra-high-speed operation, Nasvytis tested a 3.7-kW (5-hp), three-row, 120-to-1 ratio speed increaser (ref. 3). The drive was preloaded and operated without torque at 480 000 rpm for 15 minutes and ran for 43 consecutive hours at 360 000 rpm without lubrication but with air cooling. Two back-to-back drives were operated for 180 hours at speeds varying from 1000 to 120 000 rpm and back to 1000 rpm. They transmitted between 1.5 and 2.2 kW (2 and 3 hp, ref. 3). Another 3.7-kW (5-hp), three-row speed increaser, with a speed ratio of 50, was tested for more than 5 hours at the full rated speed of 150 000 rpm with oil mist lubrication and air cooling. It successfully transmitted 3.7 kW (5 hp) at 86 percent efficiency (ref. 3).

Smooth, quiet, high-speed operation are inherent qualities of the Nasvytis Multiroller Traction Drive concept. These qualities make it attractive for high-ratio speed reducer applications such as those associated with high-speed, gas-turbine prime movers.

The research reported herein was conducted to determine (1) key operational and performance factors of a high-speed, high-ratio Nasvytis Multiroller Traction Drive, such as drive efficiency, roller creep, lubrication requirements, temperature distribution, and roller cluster stability and (2) the effect of design traction coefficient on these operational characteristics over a wide range of speed and torque. Parametric tests were conducted on a back-to-back transmission test stand with 14.7-to-1 fixed-ratio Nasvytis Multiroller Traction Drives. Test parameters included speeds to 73 000 rpm and input power levels to 127 kW (170 hp). A synthetic, cycloaliphatic traction fluid was used as the test lubricant.

## TEST DRIVE, TEST STAND, AND PROCEDURE

### Test Drive

The Nasvytis Multiroller Traction Drive tested in this study is shown in figure 1. The test drive is a single-stage planetary configuration with two rows of five stepped planet rollers contained between the concentric sun and ring rollers. Either the sun or ring roller may act as the input or output member. Reaction torque is carried to the housing by a pair of rolling-element ball bearings installed in the second (outer) row of planet rollers. The first (inner) row of planet rollers and the sun roller require no bearings, so that the number of total drive bearings is greatly reduced. The reaction torque bearings are located in the optimum position, the outer planet-roller row, where the reaction forces and operating speeds are relatively small. The ring-roller assembly is positioned by its contact with the second row of planet rollers and is splined to the low-speed input-output shaft.

Because the planet rollers in the test drive are the three-point contact with adjacent rollers, the roller cluster has a high degree of stability: The first row of planet rollers and the second row of planet rollers (to the extent of bearing internal clearance) will shift under load until a nearly ideal force balance is established. Consequently, slight mismatches in roller dimensions, housing distortions under load, or thermal gradients will have little effect on drive performance other than to cause a slight change in roller orientation. From a roller manufacturing standpoint this roller cluster flexibility will accommodate rather crudely matched rollers. Differences between contacting roller diameters as great as approximately  $\pm 0.02$  mm ( $\pm 0.0008$  in.), several times those of ordinary mass-produced roller bearings, should cause few, if any, operational difficulties.

The number of planet-roller rows, the number of planet rollers in each row, and the relative diameter ratios at each contact are variables to be optimized according to the overall speed ratio and the uniformity of contact forces. In general, drives with two planet rows are suitable for speed ratios to about 25, and drives with three planet rows are suitable for ratios to about 150. For the nominal design speed ratio of 14.7, two rows of five planet rollers each were selected. The speed ratios across the contacts between the sun roller and the first row of planet rollers, between the first and second rows of planet rollers, and between the second row of planet rollers and the ring roller were 1.28, 3.87, and 2.97, respectively, for a total speed ratio of 14.7.

The test drives were equipped with a loading mechanism that automatically adjusted the normal contact load between the rollers in proportion to the transmitted torque. This mechanism operated above some preselected, minimum preload setting. The automatic loading mechanism insured that the ratio of traction forces to normal con-

tact forces, or the design traction coefficient  $\mu^*$ , was constant under all operating conditions. The loading mechanism consisted of eight 6-mm by 6-mm rollers contained in wedge-shaped cam pockets on the outboard side of each ring roller (fig. 1). The inside diameters of the two-piece ring-roller set were slightly tapered. This taper caused the drive cluster to be radially loaded when the cam rollers squeezed the ring-roller halves axially together under torque.

The design traction coefficient  $\mu^*$  could be varied by simply changing the slope of the wedge-shaped cam pockets. In this investigation, three values of  $\mu^*$  (0.039, 0.048, and 0.057 at the contact between the sun roller and the first row of planet rollers) were examined.

The ring roller and the planet rollers were manufactured from consumable vacuum-melted (CVM) SAE-9310 steel that was case carburized to a Rockwell-C hardness of 60 to 63. The sun roller was made of through-hardened, CVM AISI-52100 steel with a Rockwell-C hardness of 61 to 63. All roller running surfaces were ground to surface finishes from 0.1 to 0.2  $\mu\text{m}$  (4 to 8  $\mu\text{in.}$ ) rms. The remaining drive components and structure were fabricated from low-carbon steel.

The test drives were sized to transmit 149 kW (200 hp) continuously although test-stand power limitations restricted testing to 127 kW (170 hp). They had transient overload capability of 261 kW (350 hp), based on yielding stress considerations.

Each test drive was approximately 25 cm (10 in.) in diameter with a main-body length of approximately 11 cm (4.3 in.). The rotating drive components weighed 87 N (19.7 lb). An extra-stiff, welded steel housing added 170 N (38.6 lb) to the total weight of each drive. It is estimated that about 35 percent of this structural weight could be saved by using a cast aluminum housing. With a cast aluminum housing, which would be used in a production drive, the weight-to-power ratio for the test drive would be 0.76 N/kW (0.13 lb/hp) on a transient basis and 1.34 N/kW (0.22 lb/hp) on a maximum, continuous basis.

#### Lubricant

The test lubricant used in this study was a synthetic, high-traction cycloaliphatic hydrocarbon fluid. Its traction coefficient is approximately 50 percent greater than those of conventional mineral oils (ref. 2). This fluid exhibited good fatigue-life performance in the tests of reference 8. Its properties are given in table I.

#### Test Stand

The NASA fixed-ratio, traction-drive test stand uses the back-to-back or recirculating-power principle, which permits accurate efficiency measurements to be

made (typically within  $\pm 0.3$  percent as compared with  $> \pm 1$  percent with input-output torque meters). A schematic of the test stand is shown in figure 2. Two drives with individual lubrication systems were tested concurrently. The high-speed shafts of these drives were directly coupled by a high-speed, flexible gear-coupling. The low-speed shafts were coupled by parallel-shaft stand gearboxes that were individually connected to the case and rotor of a hydraulic torque motor. The hydraulic motor loaded the gearboxes and test drives when it was pressurized through the oil supply housing (hydraulic slip ring). The torque level in the test drives was controlled by a closed-loop, servocontrol system that regulated the pressure difference across the hydraulic motor through a servocontrol valve. When the drive motor rotated the hydraulically loaded test drives, a power flow was established in the closed loop in which one transmission acted as a speed increaser and the other as a speed reducer. The drive motor supplied only the power required to rotate the test drives and test-stand gearboxes under the test load. This power was equal to the total test-stand power losses.

Efficiency was measured by comparing the total test-stand power losses when the test drives were in place with the test-stand tare power losses when the test drives were removed, at the same test conditions. The test-stand tare power losses were measured under load by replacing the test drives with a dummy shaft. With this technique, peak efficiency can be determined accurately to within  $\pm 0.3$  percent. Drive-motor input torque and loop torque at the speed reducer's output shaft were measured with rotary transformer torque meters.

Speeds were accurately measured with magnetic and proximity probe pickups to one part in 10 thousand at test-drive input and output shafts so that the small changes in speed ratio due to creep (slight relative motion between driving and driven rollers) could be detected.

Temperatures of the lubrication oil into and out of the test drives and the test-stand gearboxes were recorded. Input oil temperatures were maintained by an automatic controller. Sun-roller temperatures were measured approximately by placing a thermocouple junction less than 0.3 cm (0.1 in.) above the roller surface. The inner-race temperature of the second row of planet rollers and outer-race temperature of the low-speed shaft bearing were measured by imbedding thermocouples in copper plugs in contact with these races. Skin temperatures of both drives and the stand gearboxes were also recorded.

Pressures of the lubrication and hydraulic torque meter systems were measured with strain-gage pressure transducers. Oil flow rates were measured with turbine flowmeters. Triaxial accelerometers were mounted on the test drives to detect abnormal vibration during the test and to perform cursory vibration analysis.

Sun- and ring-roller radial and axial positions were monitored during the tests with eddy-current proximity probes. The test drives' lubrication system consisted of



an 11-liter (3-gal) sump, a pressure pump, an oil heater and cooler, 3- $\mu$ m absolute supply and return filters, and a scavenge pump to keep the drive housing relatively dry.

### Test Procedure

Before each test the test drives were completely disassembled and the components were cleaned in an ultrasonic vapor degreaser to insure maximum cleanliness. Also, the lubricant in the test drives' lubrication systems was circulated for several hours through 3- $\mu$ m absolute filters. After the transmissions were reassembled and the minimum preload adjusted, the high-speed shafts of the two test drives were alined in a mounting fixture and coupled by a lightweight, high-speed gear-coupling.

The tests reported herein were parametric tests. The parameters that were maintained constant throughout the tests are listed in table II. Increaser input speeds were 830, 1660, 2770, 3870, and 5000 rpm; and reducer output torques were 23, 57, 85, 113, 141, 181, 226, and 282 N-m. The test procedure was to set a speed and then to increase the torque level stepwise to the required test condition. When the maximum torque level was attained, the next increment of speed was set and the procedure was repeated. To insure steady-state readings, typically 45 to 60 minutes of running was required between speed changes and 5 to 15 minutes between torque changes.

## RESULTS AND DISCUSSION

### Effects of Speed and Torque on Drive Efficiency

The effects of speeds to 73 000 rpm and input torques to 285 N-m (2520 in-lb) on multiroller-traction-drive power loss are presented in figure 3 for a design traction coefficient of 0.048. With recirculating-power test systems it is not feasible to directly measure individual test-drive power loss, so an average power loss per drive is normally assumed. However, a better estimate of increaser and reducer drive performance can be obtained by splitting the total power loss for both drives in proportion to the relative heat transferred to the cooling oil and convected through the housing. A sample calculation using this heat-loss balance is given in appendix A. With this technique the reducer generally had a slightly higher power loss than the increaser. However, as discussed later in this section, these differences in power loss have a much smaller effect on relative test-drive efficiency.

It is apparent from figure 3 that the test-drive power loss was mildly dependent on torque and significantly dependent on speed. In fact, an increase in speed caused a nearly linear increase in power loss, as illustrated in figure 4, where the torque loss at the input shaft for the test drives is plotted against input speed for two input torques.

The torque loss was nearly constant over the operating speed range and varied only slightly with input torque. This variation in torque loss with speed and load is quite similar to that of spur gears (ref. 9) and to that of traction-drive contacts (ref. 5).

Because speed seems to have little overall effect on mechanical efficiency at constant torque (fig. 5), the windage losses were probably relatively small. However, mechanical efficiency did improve with an increase in transmitted torque, with efficiency levels rising to approximately 95 percent for both increaser and reducer at the highest torque level tested. The upward trend of these performance curves shows that slightly higher efficiencies might have been attained had not the torque limit of the test stand been reached.

Figure 6 shows the variation in test-drive efficiency with input power. Both increaser and reducer appeared to have nearly the same overall efficiency, except at the two lowest operating speeds. At low speeds, the small power differences between the drives ( $\sim 0.5$  kW (0.7 hp)), as shown in figure 3, resulted in about a 2- to 3-percentage point efficiency advantage for the increaser. However, these differences in efficiency are probably not significant because of the inaccuracies associated with the heat-balance technique at these lower power levels.

It is clear from figure 6 that, for best efficiency at any required horsepower, the traction drive should be operated at the lowest possible speed since this will require the highest possible torque (fig. 5). This is the most efficient way of operating most mechanical and hydraulic drive systems as well as most internal combustion engines. However, the efficiency advantages of operating for prolonged times at high torque levels might be offset by a reduction in drive-system fatigue life.

Unlike gear-to-gear contacts, the exact speed ratio across a traction contact is not independent of torque. A small speed difference will exist between lubricated, elastic, rolling bodies under torque transmission. This difference is due to the combination of tangential, elastic deformation of the roller material (ref. 10) and the viscoelastic straining of the lubricant's elastohydrodynamic film (ref. 11). As long as the peak traction coefficient of the lubricant within the contact is not exceeded, this relative motion will be a very small percentage (typically  $< 0.5$  percent for cylindrical contacts) of the contact's rolling velocity. This small relative motion is commonly referred to as creep. The traction performance of lubricants is usually given in the form of traction-coefficient-versus-creep curves. The traction coefficient is generally a linear function of the creep rate below approximately 75 percent of the peak traction coefficient. Above this value the traction coefficient rapidly levels off with an increase in creep rate as nonlinear viscoelastic effects become important. At high creep rates, thermal effects cause a reduction in traction coefficient until gross slip, or 100 percent creep, is reached. To insure against gross slip, it is common design practice to keep the design traction coefficient somewhat less than 75 percent of the anticipated maxi-

mum available traction coefficient at the required operating conditions.

The creep rate also represents a loss in power that is equal to the product of the speed difference and the transmitted torque. This can be expressed in terms of speed efficiency  $\eta_s$ , which is defined as follows:

$$\eta_s = \frac{\text{Measured output speed}}{\text{Design output speed}}$$

Figure 7 shows that speed and load have little effect on the measured speed efficiency of the test drives. The speed efficiencies presented are accurate to  $\pm 0.05$  percent. Speed efficiencies in excess of 98.6 percent were recorded for both test drives. Thus the total creep rate across three traction contacts was held to less than 1.4 percent by the automatic loading mechanism.

All remaining power losses, apart from the creep power loss, can be expressed in terms of torque efficiency  $\eta_t$ , which is defined as follows:

$$\eta_t = \frac{\eta_o}{\eta_s}$$

where  $\eta_o$  is the overall model efficiency. Torque efficiency plots for the test drives are given in figure 8. Because of the high values of  $\eta_s$ , these curves are quite similar to those of figure 5.

In general, traction-drive torque efficiency is a measure of the power losses due to contact misalignment, spin (for contacts with tapered or varying transverse curvatures), rolling resistance, and miscellaneous drive losses. Miscellaneous drive losses, such as windage and support-bearing tare losses, can become a significant portion of the total power loss, particularly at light loads.

#### Effects of Design Traction Coefficient on Drive Efficiency

The geometry of the wedge-shaped cams in the automatic loading mechanism was varied to study the effects of design traction coefficient  $\mu^*$  on traction-drive efficiency. As shown in figure 9, the three design traction coefficients tested had little effect on performance. Nor did these three values of  $\mu^*$  have any significant effects on any other operating variable, such as roller temperatures or speed efficiency. However, both test drives, when operated with the 0.057-percent-design-traction-coefficient cams, did show some signs of impending slip at sun-roller speeds above 57 500 rpm at high torque levels. It is well known that the available traction coefficient  $\mu$  will decrease with an increase in rolling velocity. Apparently, at the high surface speeds of the sun roller ( $\geq 85$  m/sec (16 700 ft/min)), the available coefficient of traction  $\mu$  for

the traction lubricant - contact combination approaches 0.057, the value of the design traction coefficient  $\mu^*$ . This would suggest using a lower value of  $\mu^*$ , that is, applying more normal load, to insure against gross slip. On the other hand, using too low a value of  $\mu^*$  would greatly increase the normal load acting on the contact and thereby adversely affect fatigue life and possibly part-load efficiency.

#### Effects of Speed and Torque on Temperature

Operating speed, as shown in figures 10 to 12, had a far greater effect than torque on the operating temperature of components in the test drives. Varying sun-roller speed from 12 000 rpm to 73 000 rpm at constant torque increased sun-roller absolute temperatures by 12 to 17 percent. However, varying sun-roller torque from 2 N-m to 20 N-m (18 in-lb to 180 in-lb) at constant speed caused only a 2 to 4 percent variation. This observation is consistent with the far-more-dominant effect of speed on power loss, as discussed earlier (fig. 4).

Although the hollow sun roller was cooled effectively by lubricant that flowed under the contact surface and out through radial holes, contact temperatures - as measured by thermocouples just above the contact surface - approached 422 K (500<sup>o</sup> F) at maximum speed. This temperature is the practical operating-temperature limit for drive components made from AISI 52100 steel. The reason is that above this temperature AISI 52100 steel experiences a significant reduction in hardness, which would adversely affect fatigue life (ref. 12). A bearing steel with good hot-hardness retention, such as AISI M-50, is recommended for prolonged sun-roller speeds above 73 000 rpm. The average temperatures of the planet-bearing inner race (fig. 11) were only about 22 K (40 deg F) above the oil inlet temperature at the maximum test conditions.

The sun roller, planet bearings, and housing of the reducer seemed to operate slightly cooler (<3 percent on an absolute temperature basis) than the corresponding components in the increaser (figs. 10 to 12). The temperature differences were relatively small, in part because of the slightly lower reducer oil inlet temperature (~3 K (5 deg F)).

The effects of input power and operating speed on the temperature rise across the cooling oil are shown in figure 13. As would be expected from the power-loss measurements, a change in operating speed had a greater effect on oil temperature rise than did a change in transmitted torque.

The oil temperature rises of the reducer and increaser were comparable at sun-roller test speeds above 40 500 rpm. However, at lower test speeds, the reducer's oil temperature rise was approximately 2 K (3.5 deg F) greater than the increaser's at 12 000 and 24 000 rpm. These differences are indicative of slightly, but not signif-

icantly, higher power losses for the speed reducer as calculated from the heat-balance analysis detailed in appendix A and depicted graphically in figure 4.

### Roller Motions

As previously mentioned, the sun roller and first row of planet rollers are free floating and rely on contact with adjacent rollers for location. Radial positioning of the roller cluster depends primarily on the location and spacing of the reaction bearings in the second-row of planet rollers. Little, if any, positioning is provided by the ring roller through its spline connection with the low-speed input-output shaft. Multiroller-cluster radial stability is discussed in detail in reference 3.

Axial roller stability of the sun roller and the first row of planet rollers was provided by special, tapered, convex-concave roller contacts that were designed in accordance with the criteria of reference 13. These contoured surfaces greatly minimized axial roller motions without the need for roller flanges as an axial restraint. Roller flanges not only are susceptible to damage from high differential sliding velocities, but also are a source of appreciable power loss.

Proximity probes were installed in the test drives to monitor roller motions under a variety of operating conditions. External proximity probes were located radially at the neck of the sun roller near the coupling, and internal probes were located axially at the end of the sun roller. The first and second rows of planet rollers operated very stably (less than 0.05-mm (0.002-in.) peak-to-peak motion) throughout most of the parametric tests. Representative time traces of sun-roller motions at a nominal speed of 56 500 rpm are shown in figure 14. Total peak-to-peak motions were 0.10 and 0.15 mm (0.004 and 0.006 in.) radially and 0.05 and 0.10 mm (0.002 and 0.004 in.) axially for the increaser and reducer, respectively.

The increaser's sun roller operated very smoothly, but the reducer's sun roller exhibited some minor oscillations at the low-speed output-shaft frequency of 65 Hz. These oscillations are probably due to slight misalignment (approximately  $0.08^\circ$ ) between the ring-roller axis and the output-shaft axis. This causes the drive cluster to cock slightly and to nutate at the output-shaft speed. Subsequent measurements of axial motion at the ring-roller face confirmed this hypothesis. Improvement in the alignment and piloting of the reducer's ring-roller spline should alleviate much of this motion.

The high-frequency oscillations shown in figure 14 occur at a sun-roller rotational frequency of approximately 940 Hz. The radial motions at this frequency are largely due to unbalance of the high-speed, flexible gear-coupling together with a small amount of roller surface runout. Although the high-speed coupling was dynamically balanced on a fixture to 106 dyne-cm (0.0015 oz-in.), unavoidable misalignment between the

sun-roller spin axes and the necessary radial clearance between male and female spline teeth undoubtedly contributed to the unbalance experienced during operation. For vibration-sensitive, high-speed applications, in-place dynamic balancing techniques or more sophisticated coupling methods are recommended.

### SUMMARY OF RESULTS

Parametric tests were conducted on two high-speed, 14.7-to-1 fixed-ratio Nasvytis Multiroller Traction Drives. The test drive was arranged in a single-stage, planetary configuration with two rows of stepped planet-rollers between the concentric sun and ring rollers. It was equipped with an automatic roller-loading device that maintained a constant design traction coefficient. Two drives were tested concurrently in a back-to-back arrangement. A synthetic, cycloaliphatic traction fluid was used as the test lubricant. Test parameters included nominal sun-roller speeds to 73 000 rpm and input power levels to 127 kW (170 hp). Three design traction coefficients - 0.039, 0.048, and 0.057 - were tested. The following results were obtained:

1. The test drives operated smoothly and efficiently throughout the full range of test conditions. A nominal peak efficiency of 95 percent was measured.
2. Transmission efficiency increased with torque. The effect of operating speed on efficiency was small.
3. Varying the design traction coefficient had a relatively small effect on overall efficiency, creep rate, or operating temperatures. However, with a design traction coefficient of 0.057, the test drives showed signs of impending slip at high torque when operated at sun-roller speeds above 57 500 rpm.
4. The measured speed efficiency of the test drives exceeded 98.6 percent. Thus, the total creep rate across the three traction contacts was limited to 1.4 percent.

Lewis Research Center,  
National Aeronautics and Space Administration,  
Cleveland, Ohio, August 17, 1978,  
505-04.

## APPENDIX A

### TEST-DRIVE PERFORMANCE CALCULATIONS

#### Speed Efficiency and Creep

Creep, where the test-drive speed ratio changes with a change in torque, represents a power loss in traction drives. The definition of speed efficiency is

$$\eta_s = \frac{\text{Measured output speed}}{\text{Design output speed}} \times 100$$

Referring to figure 15(a)

$$\eta_{s,1} = \frac{S3}{S4 \times DR_1} \times 100$$

$$\eta_{s,1} = \frac{R_1}{DR_1} \times 100 \quad (A1)$$

and

$$\eta_{s,2} = \frac{S2}{\left(\frac{S3}{DR_2}\right)} \times 100$$

$$\eta_{s,2} = \frac{DR_2}{R_2} \times 100 \quad (A2)$$

Thus the speed efficiencies can be expressed as a ratio of the measured speed ratio to the design speed ratio. The design ratio is the geometric roller radius ratio under load conditions.

Creep is the percent change in the output speed from the design output speed.

$$CREEP_1 = (1 - \eta_{s,1}) \times 100 \quad (A3)$$

$$CREEP_2 = (1 - \eta_{s,2}) \times 100 \quad (A4)$$

## Power Loss

To determine efficiency in square-loop testing, the test-stand power loss when the test drives are in place is compared with the test-stand power loss when the drives are removed and replaced by a connecting dummy shaft. Referring to figure 15(b), the test-stand power losses HP7 are measured at the drive-motor input. The gearbox power losses CALHP1 and CALHP2 are determined as a function of speed and torque from calibration tests with the test drives removed. Since torque is measured only at the HP2 and HP7 locations, it is necessary to do a power flow analysis to arrive at HPLOSS.

$$\begin{aligned}
 \text{HPLOSS} &= \text{HP4} - \text{HP2} \\
 &= (\text{HP5} + \text{HP7} - \text{CALHP1}) - \text{HP2} \\
 &= (\text{HP6} + \text{HP8}) + \text{HP7} - \text{CALHP1} - \text{HP2} \\
 &= (\text{HP2} - \text{CALHP2}) + \text{HP8} + \text{HP7} - \text{CALHP1} - \text{HP2} \quad (\text{A5})
 \end{aligned}$$

$$\text{HPLOSS} = \text{HP8} + \text{HP7} - \text{CALHP1} - \text{CALHP2} \quad (\text{A6})$$

The only unknown quantity is HP8, which is found as follows:

$$\text{HP8} = K[\text{TORQ6} (\text{S5} - \text{S6})] \quad (\text{A7})$$

$$\text{TORQ6} = \frac{1}{K} \frac{\text{HP6}}{\text{S6}} = \frac{1}{K} \frac{(\text{HP2} - \text{CALHP2})}{\text{S6}} \quad (\text{A8})$$

Speed is accurately measured at S4 and S2:

$$\text{S6} = \frac{\text{S2}}{2.765} \quad (\text{A9})$$

$$\text{S5} - \text{S6} = \frac{\text{S4} - \text{S2}}{2.765} \quad (\text{A10})$$

After substituting equations (A8) to (A10) into equation (A7), the hydraulic torque-motor input power can be determined as follows:

$$\text{HP8} = \frac{(\text{HP2} - \text{CALHP2})(\text{S4} - \text{S2})}{\text{S2}} \quad (\text{A11})$$

Thus the total power loss for both units HPLOSS can be found from equation (A6) by using equation (A11) and the measured variables.



### Thermal-Power-Loss Balance

The square-loop method of testing does not provide a direct method to determine individual test-drive power loss. Often an average efficiency is assumed for both test drives based on the calculated HPLOSS. If the efficiencies of the drives are high, this will be a good approximation. If the efficiencies are low, as in part-load testing, the input power levels to each drive will be significantly different and identical efficiencies would not be anticipated. Since much of the testing reported herein was done at part-load conditions, a method of splitting the total power loss on the basis of heat rejection to the cooling oil and convection to the atmosphere was developed. It is assumed that the percentage of the total power dissipated in each test drive is in the same proportion as the percentage of total heat lost by each drive to the cooling oil and the atmosphere. Referring to figure 15(c) the thermal horsepower THP is defined as follows:

$$THP = QHP + QCONV$$

where

QHP heat rejected to cooling oil

QCONV heat convected to atmosphere

RQHP percentage of power lost in increaser

$$RQHP = \frac{THP_1}{THP_1 + THP_2} \quad (A12)$$

The power lost in the increaser is

$$HPLOS_1 = HPLOSS \times RQHP \quad (A13)$$

and that for the reducer is

$$HPLOS_2 = HPLOSS - HPLOS_1 \quad (A14)$$

### Overall Efficiency and Torque Efficiency

From the power-loss split from equations (A12) and (A13) it is now possible to obtain the overall efficiencies as follows:

$$HP4 = HP2 + HPLOSS$$

$$HP3 = HP4 - RQHP \times HPLOSS$$

$$\eta_{o,1} = \frac{HP3}{HP4} \quad (A15)$$

$$\eta_{o,2} = \frac{HP2}{HP3} \quad (A16)$$

Torque efficiency is defined as follows:

$$\eta_t = \frac{\eta_o}{\eta_s}$$

so that

$$\eta_{t,1} = \frac{\eta_{o,1}}{\eta_{s,1}} \quad (A17)$$

and

$$\eta_{t,2} = \frac{\eta_{o,2}}{\eta_{s,2}} \quad (A18)$$

where  $\eta_{s,1}$  and  $\eta_{s,2}$  are determined from equations (A1) and (A2).

#### Example Calculation

As an example, a test condition consisting of an increaser input speed of 1666 rpm and a reducer output torque of 284 N-m (2507 in-lb) are used. Refer to figure 15(b).

##### Measured quantities:

S2 = 1632 rpm  
 S3 = 24 270 rpm  
 S4 = 1666 rpm  
 TORQ2 = 284 N-m (2507 in-lb)  
 HP2 = 48.42 kW (64.9 hp)  
 HP7 = 9.97 kW (13.33 hp)

##### Derived quantities:

CALHP1 = 2.78 kW (3.72 hp)  
 CALHP2 = 2.63 kW (3.52 hp)  
 THP<sub>1</sub> = 2.81 kW (3.76 hp)  
 THP<sub>2</sub> = 3.29 kW (4.41 hp)  
 DR<sub>1</sub> = 14.69  
 DR<sub>2</sub> = 14.74

$$\eta_{s,1} = \frac{S3}{S4 \times DR_1} = \frac{24\,270}{1666 \times 14.69} = 0.992, \text{ or } 99.2 \text{ percent}$$

$$\eta_{s,2} = \frac{S2}{\left(\frac{S2}{DR_2}\right)} = \frac{1632}{\left(\frac{24\,274}{14.74}\right)} = 0.991, \text{ or } 99.1 \text{ percent}$$

$$CREEP_1 = 1 - 0.992 = 0.008, \text{ or } 0.8 \text{ percent}$$

$$CREEP_2 = 1 - 0.991 = 0.009, \text{ or } 0.9 \text{ percent}$$

$$HPLOSS = HP8 - CALHP1 - CALHP2 + HP7$$

$$= HP8 - 2.78 - 2.63 + 9.94$$

$$= HP8 + 4.53$$

$$HP8 = \frac{(HP2 - CALHP2)(S4 - S2)}{S2}$$

$$HP8 = \frac{(48.42 - 2.63)(1666 - 1631)}{1631} = 0.983 \text{ kW (1.31 hp)}$$

$$HPLOSS = 0.983 + 4.53 = 5.51 \text{ kW (7.37 hp)}$$

$$RQHP = \frac{THP_1}{THP_1 + THP_2} = \frac{2.81}{2.81 + 3.29} = 0.46$$

$$HPLOS_1 = RQHP \times HPLOSS = 0.46 \times 5.51 = 2.54 \text{ kW (3.40 hp)}$$

$$HP4 = HP2 + HPLOSS = 48.42 + 5.51 = 53.93 \text{ kW (72.11 hp)}$$

$$HP3 = HP4 - HPLOS_1 = 53.93 - 2.54 = 51.39 \text{ kW (68.71 hp)}$$

$$\eta_{o,1} = \frac{HP3}{HP4} = \frac{51.39}{53.94} = 0.953, \text{ or } 95.3 \text{ percent}$$

$$\eta_{o,2} = \frac{HP2}{HP3} = \frac{48.42}{51.39} = 0.942, \text{ or } 94.2 \text{ percent}$$

$$\eta_{t,1} = \frac{\eta_{o,1}}{\eta_{s,1}} = \frac{0.953}{0.992} = 0.961, \text{ or } 96.1 \text{ percent}$$

$$\eta_{t,2} = \frac{\eta_{o,2}}{\eta_{s,2}} = \frac{0.942}{0.991} = 0.951, \text{ or } 95.1 \text{ percent}$$

## APPENDIX B

### SYMBOLS

CALHP1	gearbox 1 power loss, kW (hp)
CALHP2	gearbox 2 power loss, kW (hp)
CREEP	test-drive creep, percent
DR	test-drive design ratio
HA	test-drive effective convective heat-transfer coefficient multiplied by surface area, kW/K (hp/ <sup>o</sup> F)
HPLOSS	total power loss in both test drives, kW (hp)
HPLOS	power loss in one test drive, kW (hp)
HP2	reducer output power, kW (hp)
HP3	reducer input power or increaser output power, kW (hp)
HP4	increaser input power, kW (hp)
HP5	shaft power level at location 5, kW (hp)
HP6	shaft power level at location 6, kW (hp)
HP7	drive-motor power, kW (hp)
HP8	torque-motor power, kW (hp)
K	constant defined in eq. (A7), $\frac{\text{kW}}{\text{N} \cdot \text{m} \cdot \text{rpm}} \left( \frac{\text{hp}}{\text{in} \cdot \text{lb} \cdot \text{rpm}} \right)$
QCONV	convective heat loss to atmosphere from test drives, kW (hp)
QHHP	heat loss to cooling oil from test drives, kW (hp)
R	measured drive ratio
RQHP	fraction of HPLOSS from increaser
STM	torque-motor rotational speed, rpm
S2	reducer output speed, rpm
S3	reducer input speed or increaser output speed, rpm
S4	increaser input speed, rpm
S5	shaft speed at location 5, rpm
S6	shaft speed at location 6, rpm

THP	thermal horsepower; includes heat loss to cooling oil and convective heat loss to atmosphere, kW (hp)
TORQ6	shaft torque at location 6, N-m (in-lb)
TR	room temperature, K ( $^{\circ}$ F)
TSRAV	average test-drive surface temperature, K ( $^{\circ}$ F)
$\Delta T$	test-drive cooling oil temperature rise, K (deg F)
$\eta_o$	overall efficiency
$\eta_s$	speed efficiency
$\eta_t$	torque efficiency
$\mu$	available traction coefficient
$\mu^*$	design traction coefficient

Subscripts:

1	increaser
2	reducer

## REFERENCES

1. Carson, Robert W.: Traction Drives Update. *Power Transmission Design*, vol. 19, no. 11, Nov. 1977, pp. 37-42.
2. Green, R. L.; and Langenfeld, F. L.: Lubricants for Traction Drives. *Mach. Des.*, vol. 46, no. 11, May 2, 1974, pp. 108-113.
3. Nasvytis, Algirdas L.: Multiroller Planetary Friction Drives. SAE Paper 660763, Oct. 1966.
4. The Planetary Friction Drive. *Prod. Eng.*, vol. 30, no. 10, Oct. 12, 1959, pp. 79-82.
5. Hewko, L. O.; Rounds, F. G., Jr.; and Scott, R. L.: Tractive Capacity and Efficiency of Rolling Contacts. *Rolling Contact Phenomena*, J. B. Bidwell, ed., Elsevier Publ. Co., 1962, pp. 157-185.
6. Hewko, L. O.: Contact Traction and Creep of Lubricated Cylindrical Rolling Elements at Very High Surface Speeds., *Trans. ASLE*, vol. 12, no. 2, Apr. 1969, pp. 151-161.
7. Hewko, Lubomyr O.: Roller Traction Drive Unit for Extremely Quiet Power Transmission. *AIAA J. of Hydronautics*, vol. 2, no. 3, July 1968, pp. 160-167.
8. Loewenthal, Stuart H.; and Parker, Richard J.: Rolling-Element Fatigue Life with Two Synthetic Cycloaliphatic Traction Fluids. NASA TN D-8124, 1976.
9. Fletcher, H. A. G.; and Bamborough, J.: Effect of Oil Viscosity and Supply Conditions on Efficiency of Spur Gearing. NEL Rep. No. 138, British Nat'l Eng. Lab., 1964.
10. Johnson, K. L.: Tangential Traction and Micro-Slip in Rolling Contact. *Rolling Contact Phenomena*, J. B. Bidwell, ed., Elsevier Publ. Co., 1962, pp. 6-28.
11. Johnson, K. L.; and Tevaarwerk, J. L.: Shear Behavior of Elastohydrodynamic Oil Films. *Proc. Roy. Soc. (London)*, Series A, vol. 356, 1977, pp. 215-236.
12. Anderson, Neil E.: Long-Term Hot-Hardness Characteristics of Five Through-Hardened Bearing Steels. NASA TP-1341, 1978. (Also AVRADCOM TR 78-16.)
13. Savage, Michael; and Loewenthal, Stuart H.: Kinematic Stability of Roller Pairs in Free-Rolling Contact. NASA TN D-8146, 1976.

TABLE I. - PROPERTIES OF SYNTHETIC CYCLOALIPHATIC

## TRACTION LUBRICANT

Additive . . . . .	Oxidation inhibitor
Kinematic viscosity, $\text{cm}^2/\text{sec}$ , at -	
244 K (-20° F) . . . . .	$31\ 600 \times 10^{-2}$
311 K (100° F) . . . . .	$23 \times 10^{-2}$
372 K (210° F) . . . . .	$3.7 \times 10^{-2}$
Flashpoint, K, °F . . . . .	422; 300
Fire point, K, °F . . . . .	435; 325
Autoignition temperature, K, °F . . . . .	589; 600
Pour point, K, °F . . . . .	230; -45
Specific heat at 311 K (100° F), J/kg·K; Btu/lb·°F . . . . .	2130; 0.51
Thermal conductivity at 311 K (100° F), J/m·sec·K; Btu/hr·ft·°F . . . . .	0.10; 0.060
Specific gravity at 311 K (100° F) . . . . .	0.886

TABLE II. - CONSTANT OPERATING PARAMETERS

Oil inlet temperature to increaser, K (°F) . . . . .	339 (150)
Oil inlet temperature to reducer, K (°F) . . . . .	336 (145)
Oil flow to test drives, liter/min (gal/min) . . . . .	8.33 (2.2)
Oil flow to sun rollers, liter/min (gal/min) . . . . .	5.30 (1.4)
Sun-roller jet oil pressures, kPa (psig) . . . . .	276 (40)
Oil inlet temperatures to gearbox, K (°F) . . . . .	327 (130)

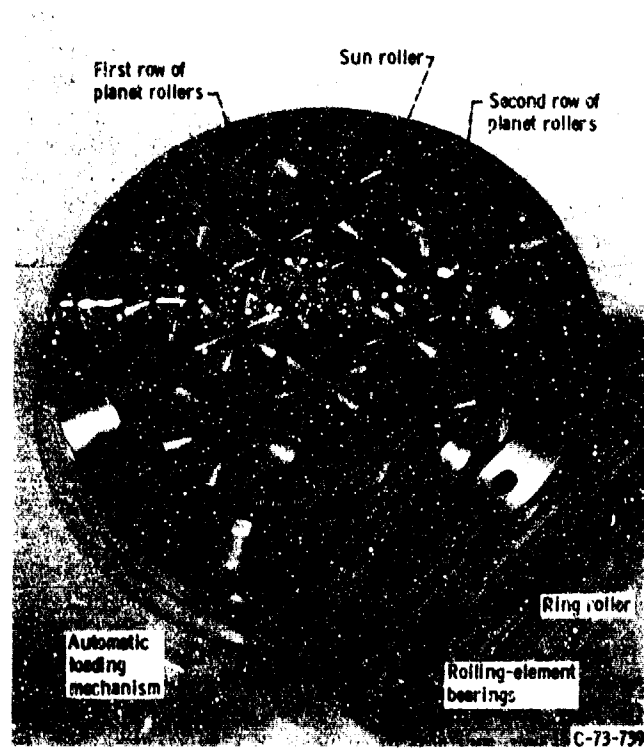


Figure 1. - Geometry of test drive.



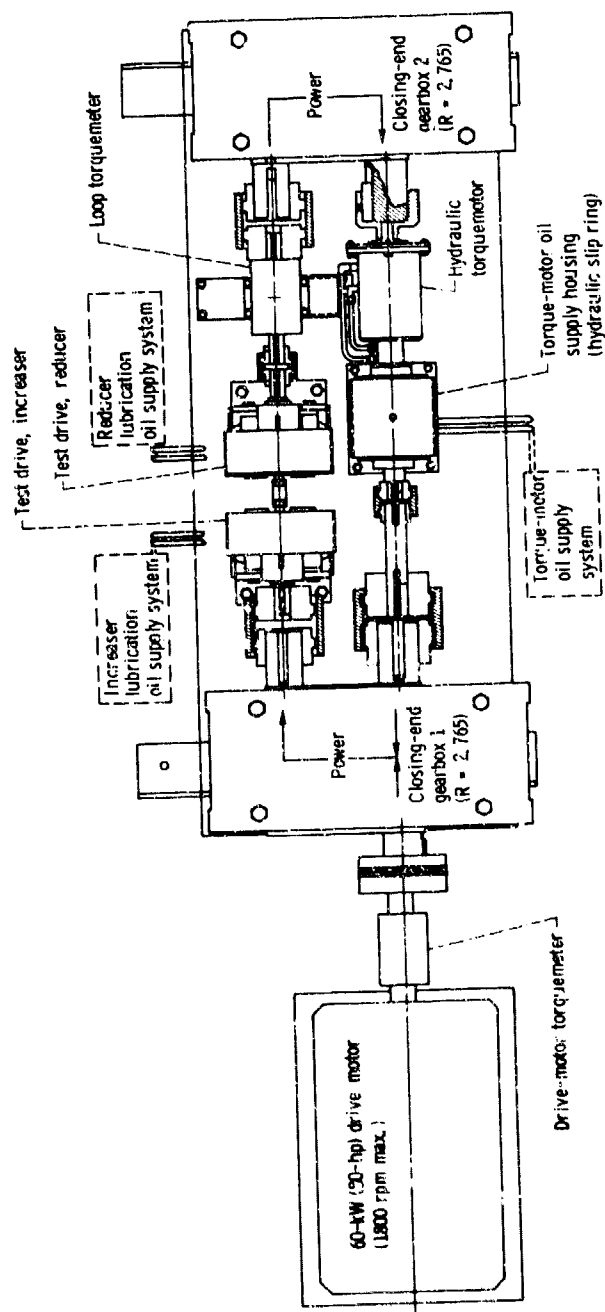


Figure 2 - Back-to-back-traction-drive test stand.

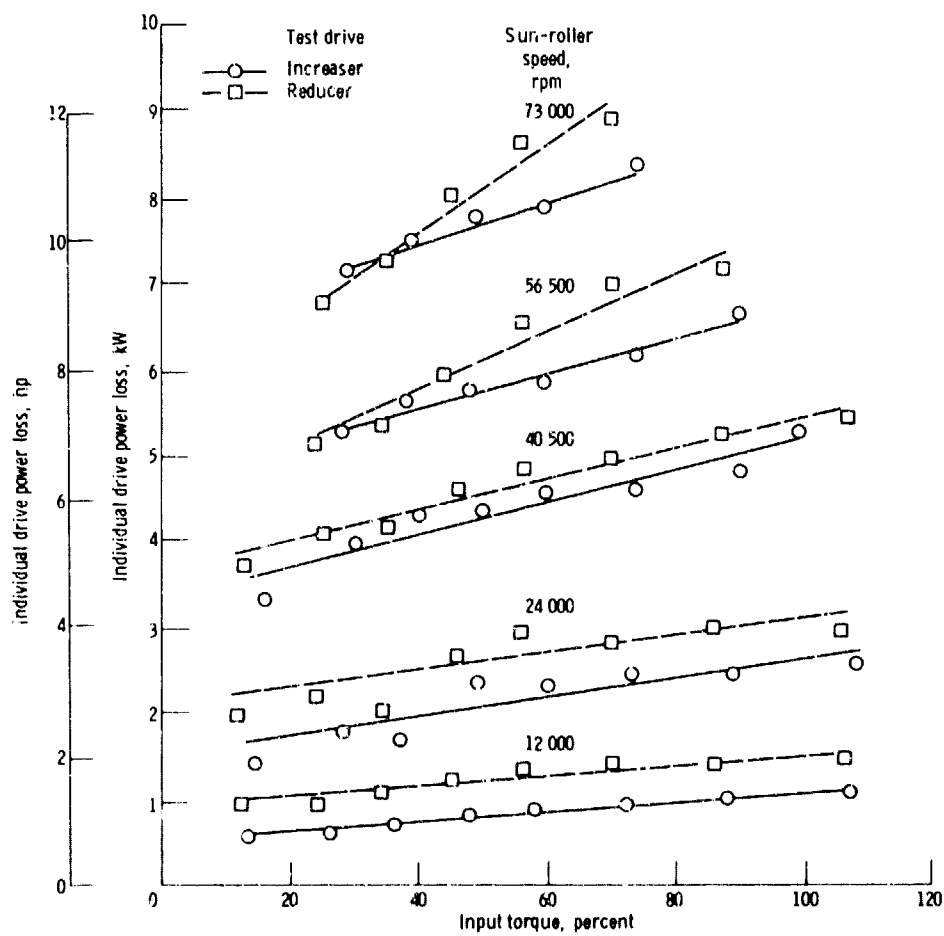


Figure 3. - Test-drive power loss as function of input torque for five input speeds. Design traction coefficient, 0.048; 100-percent input torque: 258 N-m (2520 in-lb) for increaser, 19 N-m (168 in-lb) for reducer.

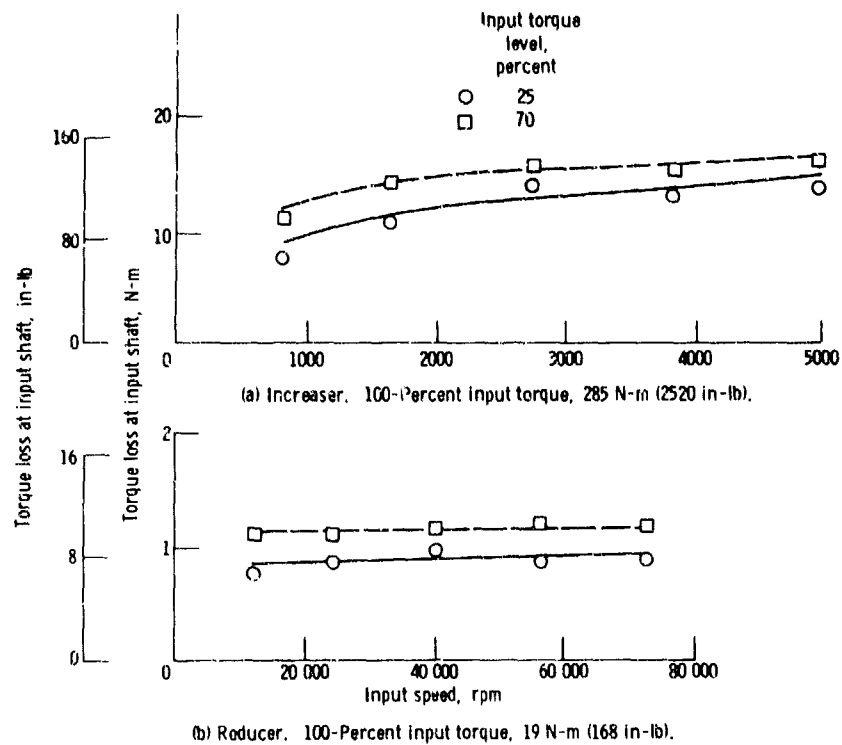
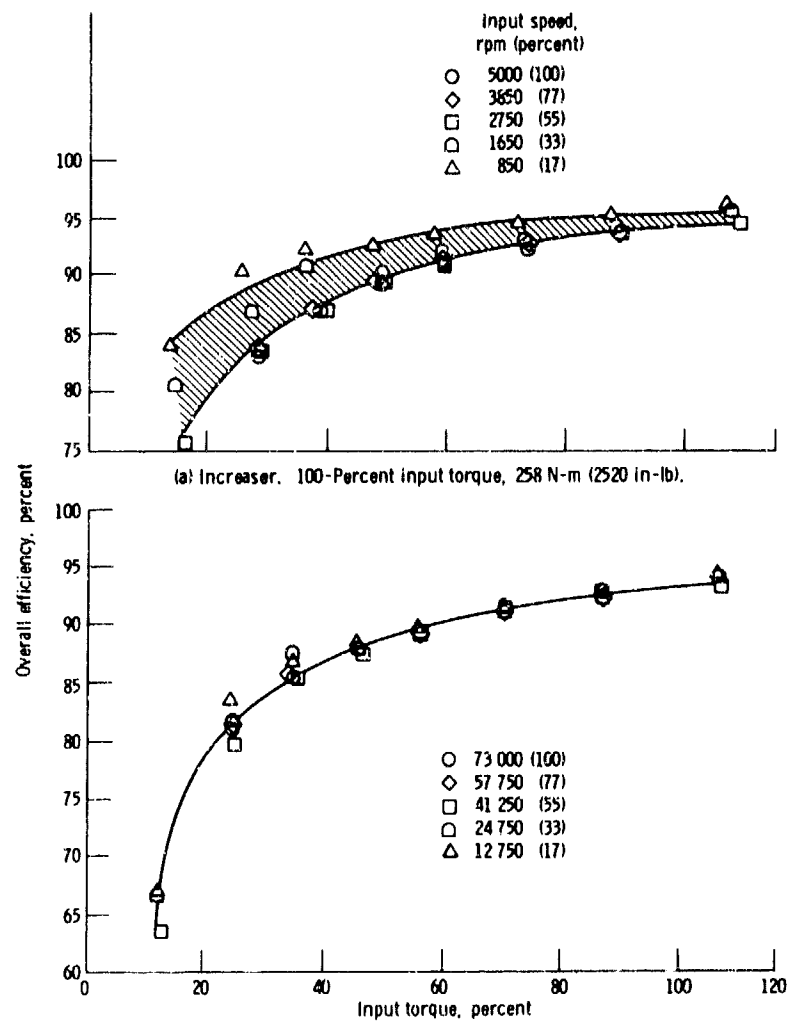


Figure 4 - Torque loss at input shaft as function of input speed for torque levels of 25 and 70 percent. Design traction coefficient, 0.048.



(a) Increaser. 100-Percent input torque, 258 N-m (2520 in-lb).  
 (b) Reducer. 100-Percent input torque, 19 N-m (168 in-lb).  
 Figure 5. - Test-drive overall efficiency as function of input torque for five input speeds. Design traction coefficient, 0.048.

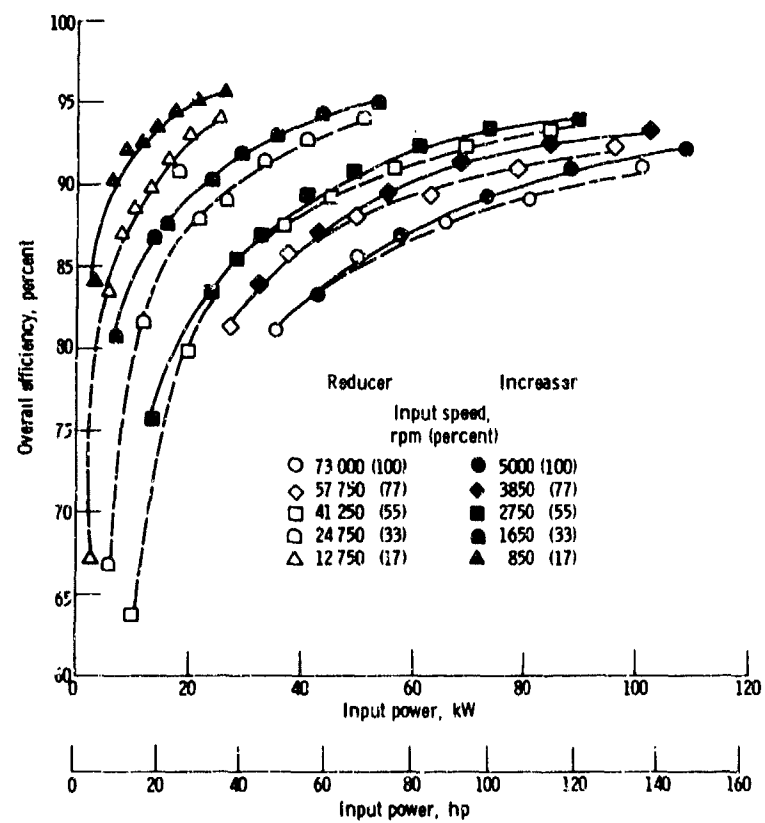


Figure 6. - Reducer and increaser test-drive overall efficiency for five input speeds. Design traction coefficient, 0.048.

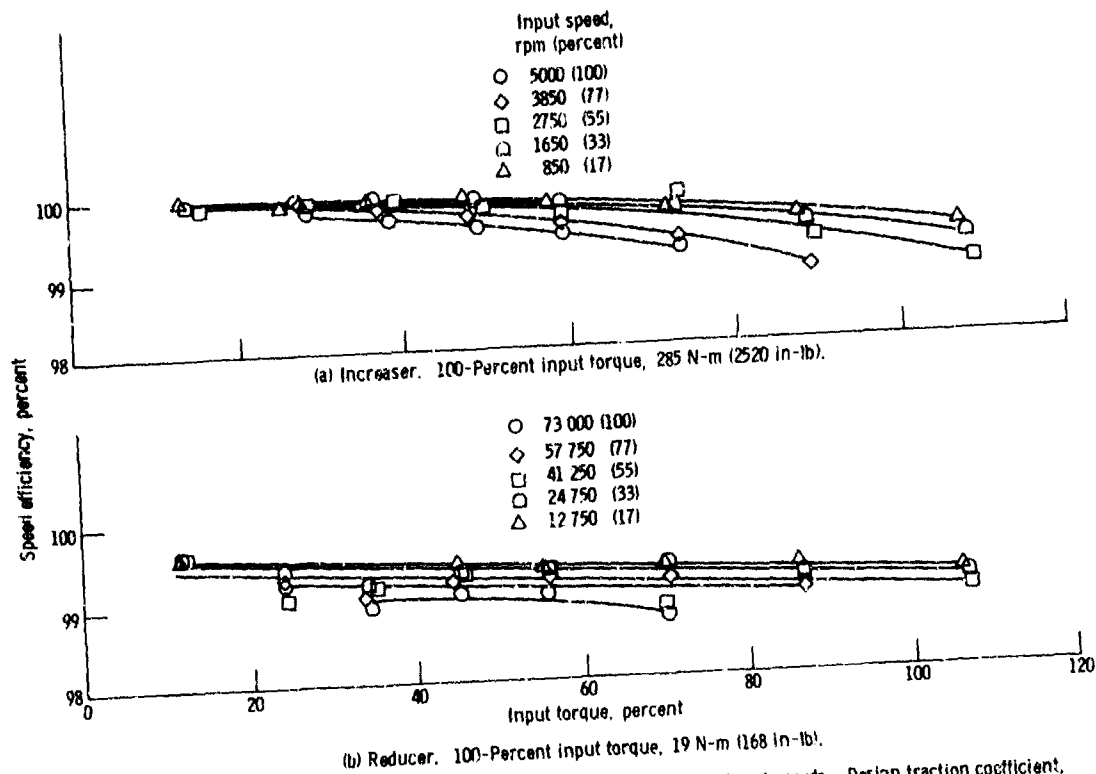


Figure 7. - Test-drive speed efficiencies as function of input torque for five input speeds. Design traction coefficient, 0.048.

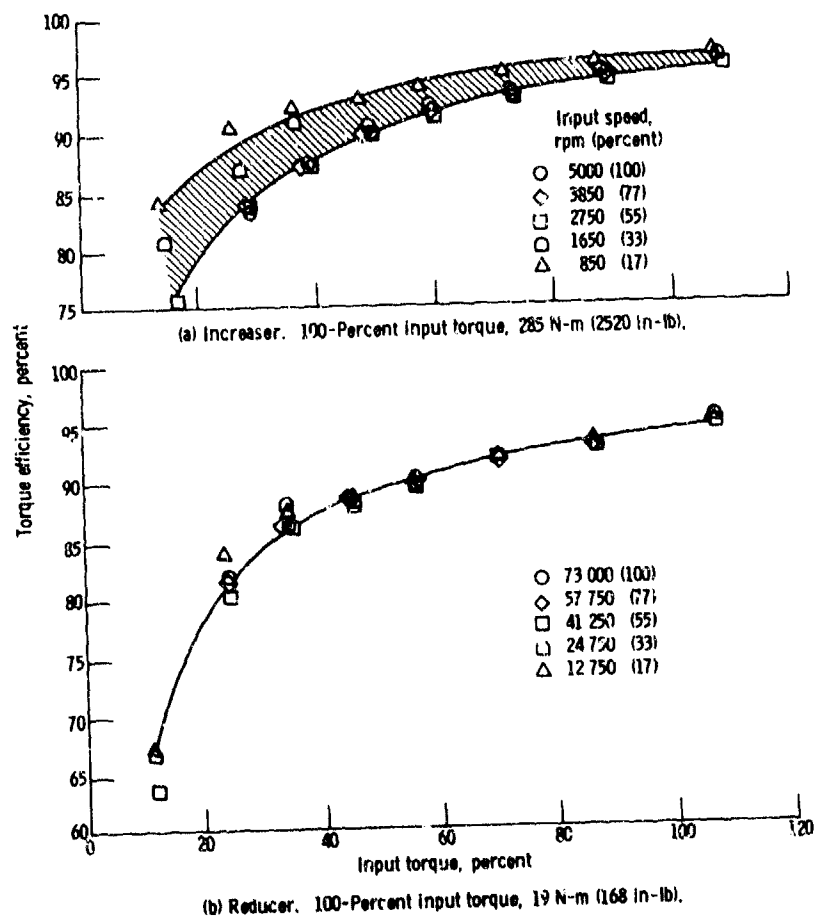


Figure 8. - Test-drive torque efficiency as function of input torque for five input speeds.  
Design traction coefficient, 0.048.

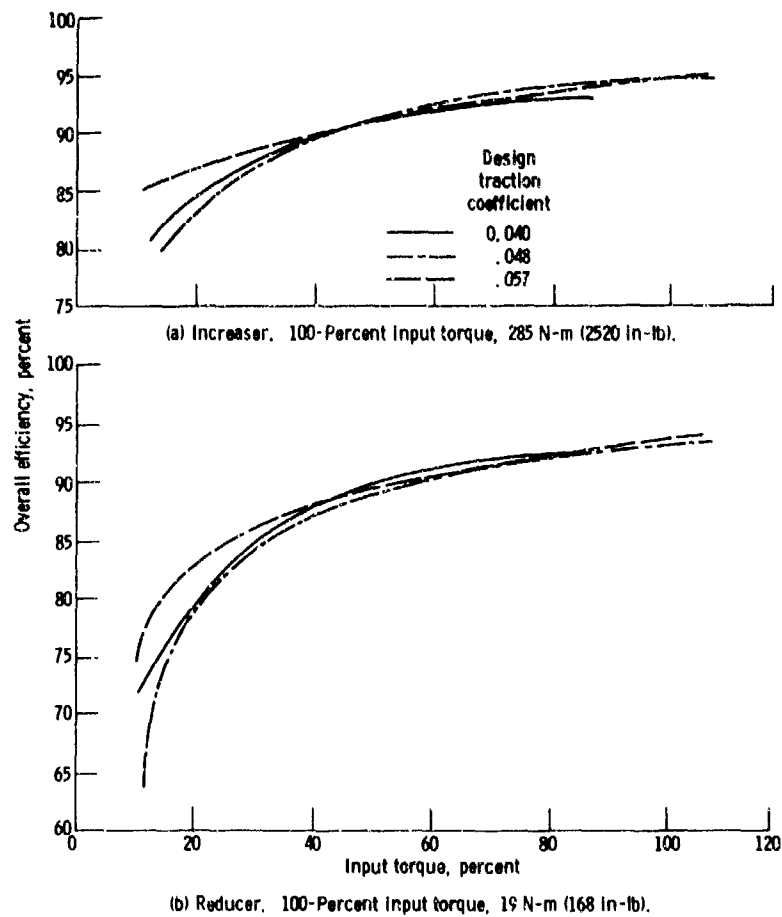


Figure 9. - Test-drive overall efficiency as function of input torque for three design traction coefficients.



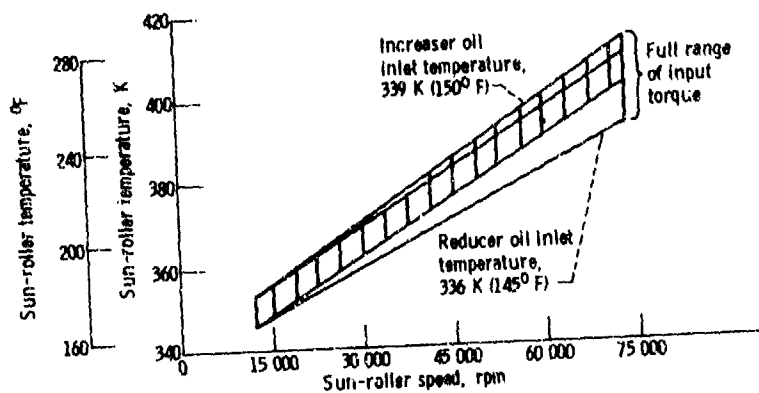


Figure 10. - Sun-roller surface temperature as function of sun-roller speed and torque. Design traction coefficient, 0.048; sun-roller oil flow rate, 5.3 liters/min (1.4 gal/min).

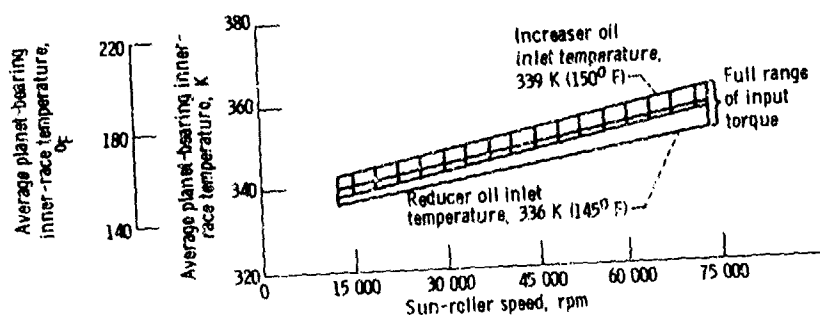


Figure 11. - Average planet-bearing inner-race temperature as function of sun-roller speed and torque. Design traction coefficient, 0.048; bearing oil flow rate, 2.5 liters/min (0.65 gal/min).

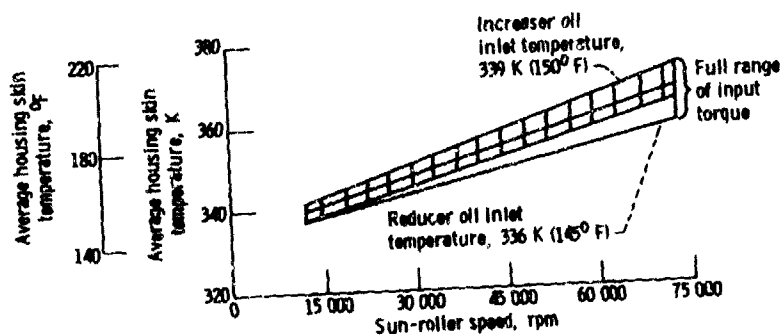


Figure 12. - Housing skin temperature as function of sun-roller speed and torque. Design traction coefficient, 0.048.

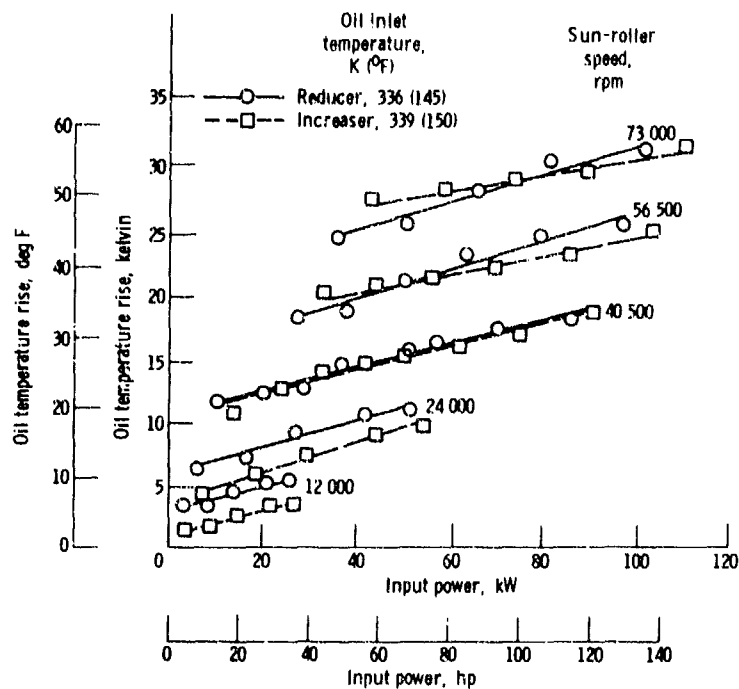


Figure 13. - Oil temperature rise (difference between oil outlet temperature and oil inlet temperature) as function of input power for five input speeds. Design traction coefficient, 0.048; total oil flow rate per drive, 8.3 liters/min (2.2 gal/min).

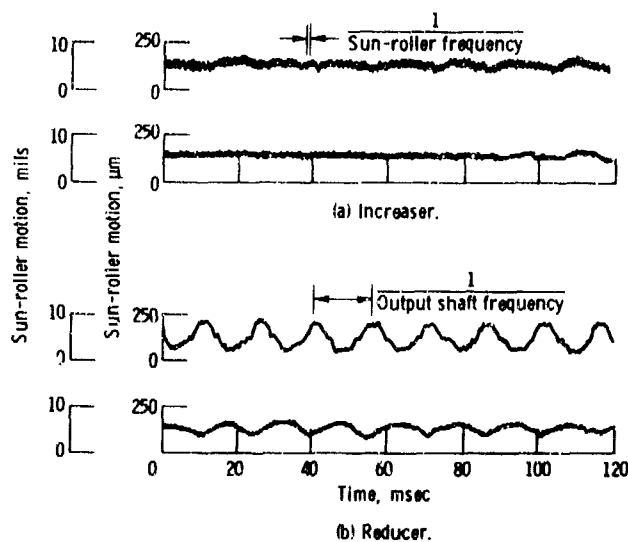


Figure 14. - Representative sun-roller motions. Sun-roller speed, 56 500 rpm; reducer output-shaft torque, 84.7 N-m (750 in-lb).

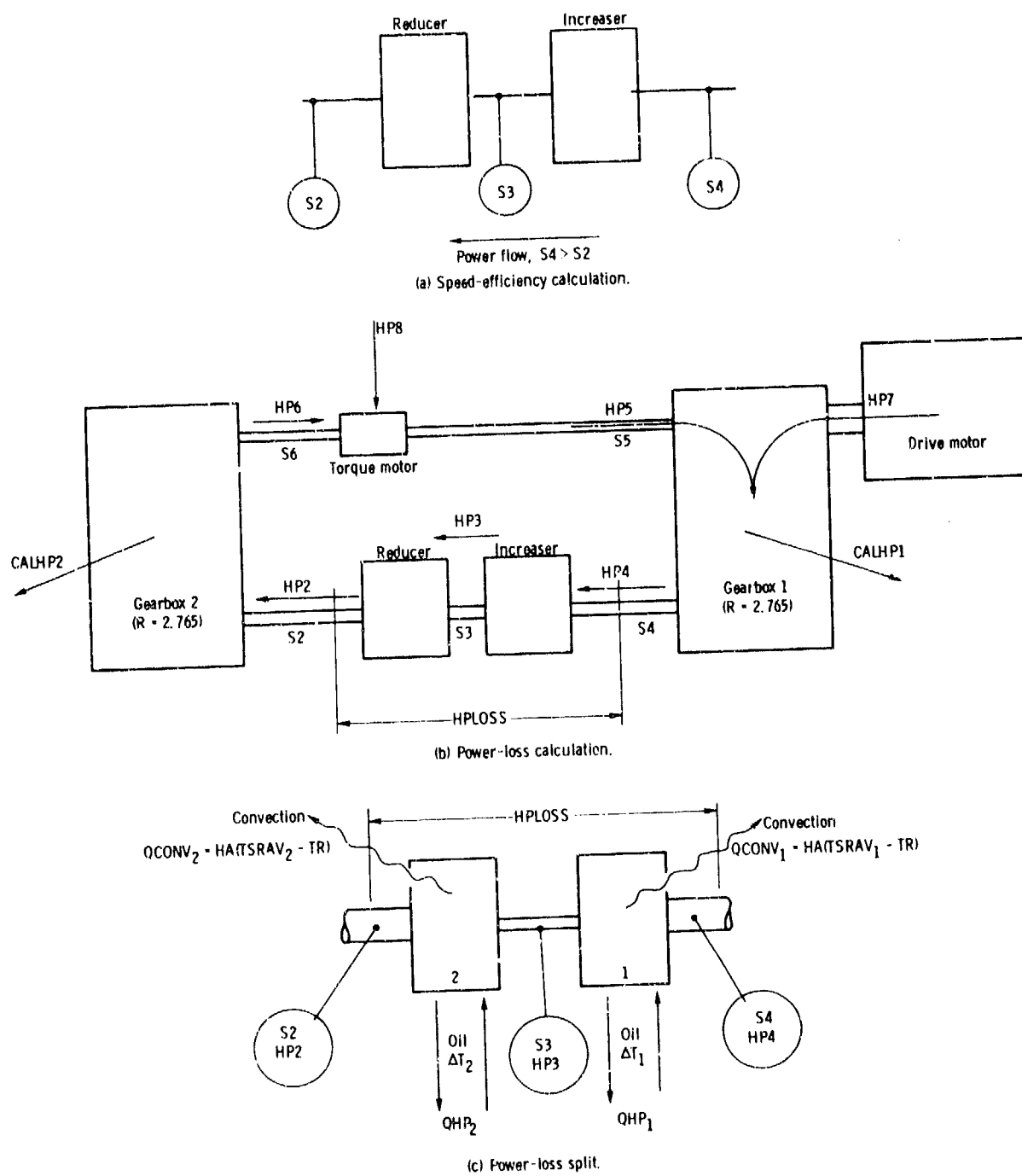


Figure 15. - Test-drive performance calculation diagrams.

1. Report No. <b>NASA TP-1378 AVRADCOM TR 78-36</b>		2. Government Accession No.		3. Recipient's Catalog No.	
4. Title and Subtitle <b>PERFORMANCE OF A NASVYTIS MULTIROLLER TRACTION DRIVE</b>				5. Report Date <b>November 1978</b>	
				6. Performing Organization Code	
7. Author(s) <b>Stuart H. Loewenthal, Neil E. Anderson, and Algirdas L. Nasvytis</b>				8. Performing Organization Report No. <b>E-9632</b>	
9. Performing Organization Name and Address <b>NASA Lewis Research Center and AVRADCOM Research and Technology Laboratories Cleveland, Ohio 44135</b>				10. Work Unit No. <b>505-04</b>	
				11. Contract or Grant No.	
12. Sponsoring Agency Name and Address <b>National Aeronautics and Space Administration Washington, D.C. 20546 and U.S. Army Aviation Research and Development Command, St. Louis, Mo. 63166</b>				13. Type of Report and Period Covered <b>Technical Paper</b>	
				14. Sponsoring Agency Code	
15. Supplementary Notes <b>Stuart H. Loewenthal, Lewis Research Center; Neil E. Anderson, AVRADCOM Research and Technology Laboratories; Algirdas L. Nasvytis, Transmission Research, Inc., Cleveland, Ohio.</b>					
16. Abstract  Tests were conducted to determine the operational and performance characteristics of a high-speed, 14.7-to-1 fixed-ratio Nasvytis Multiroller Traction Drive at speeds to 73 000 rpm and power levels to 127 kW (170 hp). The test drive was arranged in a single-stage, planetary configuration with two rows of stepped planet rollers contained between concentric sun and ring rollers. It was lubricated with a traction fluid. Two drives were tested concurrently in a back-to-back arrangement. They exhibited good performance and operated smoothly, with a nominal peak efficiency of 95 percent. Variations of the design traction coefficient imposed by the automatic roller-loading device of 0.039, 0.048, and 0.057 seemed to have relatively little effect on any of the operating variables.					
17. Key Words (Suggested by Author(s))  <b>Traction drives                      Transmissions Traction                                Drives Traction fluid Traction lubricant</b>				18. Distribution Statement  <b>Unclassified - unlimited STAR Category 37</b>	
19. Security Classif. (of this report)  <b>Unclassified</b>		20. Security Classif. (of this page)  <b>Unclassified</b>		21. No. of Pages  <b>35</b>	
				22. Price*  <b>A03</b>	

\* For sale by the National Technical Information Service, Springfield, Virginia 22161

NASA-Langley, 1978

TSARCOM  
STINFO & REF LIB